Available online at www.sciencedirect.com
ScienceDirect
Journal of Nuclear Materials 360 (2007) 32–42
journal of nuclear materials
www.elsevier.com/locate/jnucmat

Application of electrochemical techniques in pyrochemical processes – Electrochemical behaviour of rare earths at W, Cd, Bi and Al electrodes

Y. Castrillejo [a,*], R. Bermejo [a], A.M. Martínez [b], E. Barrado [a], P. Díaz Arocas [c]

[a] Departemento de Química Analítica, Facultad de Ciencias, Universidad de Valladolid, Prado de la Magdalena s/n, 47005 Valladolid, Spain
[b] Department of Materials Technology and Engineering, Sem Sælands vei 6, 7491 Trondheim, Norway
[c] CIEMAT, Dept. de Fisión Nuclear, Avda. Complutense 22, Madrid 28040, Spain

Abstract

The electrochemical behaviour of some rare earths ions (REs) – from the light to heavy lanthanides (i.e. Ce, La, Pr, Gd, Er, Ho) and Y – were investigated in the eutectic LiCl–KCl at different substrates: (i) liquid metals Cd and Bi, (ii) aluminium, and (iii) tungsten. The electrode reaction of the RE(III)/RE couples at the Cd and Bi pool electrodes was elucidated by cyclic voltammetry. The differences between the equilibrium potential adopted by a RE electrode and the $E^{r}_{1/2}$ observed with the same RE(III) solution at the liquid electrodes were consistent with the activity coefficients of RE in the liquid metal phase. The relative partial molar Gibbs energies and activities of RE in the RE–Cd and RE–Bi intermetallic compounds could be estimated by the analysis of the open circuit chronopotentiograms using Cd and Bi coated tungsten electrodes. The Gibbs energies of formation of different intermetallic compounds, as well as their molar entropies and enthalpies of formation were also calculated from the temperature dependence of the emf. The redox potential of the RE(III)/RE couples at the Al electrode was observed at more positive potentials than that at the inert electrode (W). This potential shift was explained by a lowering of the activity of the REs in the Al phases due to the formation of intermetallic compounds. Electromotive force measurements for various intermetallic compounds in two-phase coexisting states were carried out. The activities and relative partial molar Gibbs energies of REs were also obtained. Moreover, the molar entropies and enthalpies of the aluminium-rich alloys were also calculated from the temperature dependence of the emf measurements.

1. Introduction

Partitioning and transmutation (P&T) of minor actinides (MAs) and long-lived fission products (LLFP) arising out of the back-end of the fuel cycle would be one of the key-steps in any future sustainable nuclear fuel cycle. Pyrochemical separation methods would form a critical stage of P&T by recovering long-lived elements and thus reducing the radiotoxicity and volume of the nuclear wastes [1]. To this end, research and development is needed for molten salt electrorefining, electrolysis, as well as

* Corresponding author. Tel.: +34 983423000x4245; fax: +34 983423013.
E-mail address: ycastril@qa.uva.es (Y. Castrillejo).

0022-3115/$ - see front matter © 2006 Elsevier B.V. All rights reserved.
doi:10.1016/j.jnucmat.2006.08.011

reductive extraction process that are foreseen as partitioning methods for irradiated nuclear fuel such as oxide, metal and nitride fuel and high level liquid wastes [1–3].

MAs are well known to yield easily alloys with more noble elements. The deposition in an alloyed form of MAs proceeds at sensible more anodic potentials, so that their separation from other reactive elements could become easier. Then, electrolysis using Cd, Bi or Al cathodes, as well as liquid–liquid reductive extraction between molten chlorides and liquid metals, deserve an examination as possible techniques for the separation of actinides, An, from lanthanides, Ln, the most difficult fission products to separate due to their similar chemical properties [4–10].

Since the operation conditions significantly influences the feasibility of pyrometallurgical reprocessing, it is of crucial importance the knowledge of the electrochemical behaviour of An and Ln on different substrates, with and without alloy formation, for the understanding of the process, in defining efficiency of recovery and the design of the separation cell.

This work is concerned with the electrochemistry of different REs, from the light to heavy lanthanides and yttrium, which are the most difficult fission products to separate from An due to their similar properties. The study has been carried out in the eutectic LiCl–KCl at temperatures between 653 and 823 K using W, Cd, Bi and Al as substrates.

2. Experimental

Technical details about the cell used and the purification of the eutectic LiCl–KCl, may be found elsewhere [8,9]. Solutions of RE(III) were prepared by direct additions of solid $RECl_3$. In order to avoid RE–O combination, the solution is treated by bubbling HCl just before the experimental determination. All the experiments were performed under argon atmosphere.

Electrochemical measurements were performed using a PAR EG&G Model 273A potentiostat/galvanostat controlled with the PAR EG&G M270 software package. Simulated voltammograms were recorded with M271 COOL kinetic analysis software. Potentiostatic electrolysis was conducted using an AMEL Model 550 potentiostat/galvanostat provided with an AMEL Model 721 integrator.

Different working electrodes have been used: (i) liquid electrodes (i.e. Cd and Bi pools and Cd and Bi film electrodes 'CdFE' and 'BiFE'), already described in [8,9], (ii) aluminium wires of 1.0 mm in diameter and 1.0 mm thick aluminium foils and (iii) tungsten wires of 1.0 mm in diameter. Along the experiments with the Cd and Bi pool electrodes and the Al foil a graphite rood of 6.0 mm in diameter was used as counter electrode to ensure uniform current line distribution. For the other experiments a tungsten wire of 1.0 mm in diameter was used. The reference electrode was the classical Ag|AgCl ($0.75\ mol\ kg^{-1}$) contained in an end closed Pyrex tube. All the potentials are referred to this.

Auxiliary techniques such as ICP-AES, SEM, EDX and X-ray diffraction were used.

3. Results and discussion

3.1. Electrode reactions of RE(III)/RE system on Cd or Bi pool electrodes

Fig. 1 shows a representative example of the cyclic voltammograms obtained with $RECl_3$ solutions on the liquid Cd or Bi pool electrodes. Curve (1), dotted line, shows the electrochemical spectra obtained at the interface between the LiCl–KCl melt and liquid M (M = Cd or Bi) in the absence of $RECl_3$. The final rises of the voltammograms correspond to the oxidation of the electrode material, and the final descent to the reduction of Li(I) at

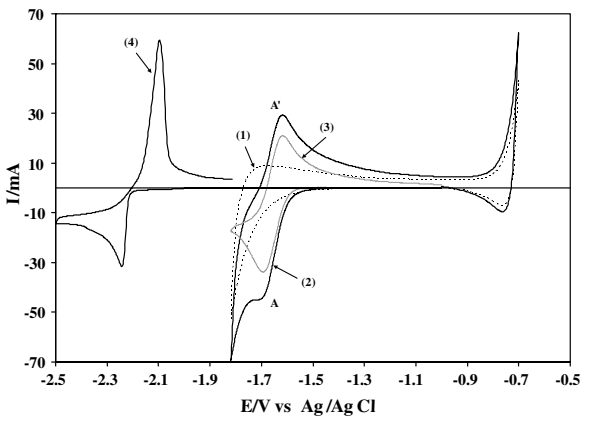

Fig. 1. Cyclic voltammograms for the reduction of a $GdCl_3$ ($9.0841 \times 10^{-5}\ mol\ cm^{-3}$) solution at a Cd pool electrode ($0.5\ cm^2$) (curves 1–3) and at a W electrode (curve 4) at 723 K and 70 mV/s. Curve (1): carried out in the absence of $GdCl_3$.

the M pool electrode [10]. Curve (2), shows the voltammogram for the redox reaction of RE(III) on the liquid metal. In order to avoid lithium deposition contribution, the current of curve (1) is subtracted from that of curve (2) as background current at the same potential, making it possible to obtain the curve (3). This background correction was made in all measurements.

Curve labelled (4) in Fig. 1, shows the cyclic voltammogram obtained with a LiCl–KCl–$RECl_3$ solution at a W electrode. The tungsten electrode was used as a reference to compare the liquid substrates because no alloys exist for the W–RE binary systems.

If the substrate is an inert material, the reaction scheme proceeds as a deposition and dissolution mechanism:

$$RE(III) + 3e \leftrightarrow RE(0). \quad (1)$$

On the contrary, at the liquid pool electrode, the voltammograms consist of a single cathodic wave A associated with an anodic wave A′ at potential values less cathodic than those obtained at the inert electrode and with the expected shape of a soluble–soluble exchange.

3.1.1. Analysis of the voltammograms obtained with a LiCl–KCl–$RECl_3$ solution using a Cd or Bi pool electrodes

As an example of the cyclic voltammograms obtained with the reported $RECl_3$ solutions, Fig. 2 shows the voltammograms obtained with a Gd(III) solution at different sweep rates, after correction of the current background, when we used Cd pool electrodes. To enable the comparison of the experimental results with the predictions of the theory an essential condition, is to maintain the concentration of RE in the Cd or Bi interphase below its solubility in the liquid metal [11]. If the amount of deposited RE exceeds its solubility, the electrode loses its homogeneity, separate solid phases would form and the voltammetric response would become less accurate and reproducible.

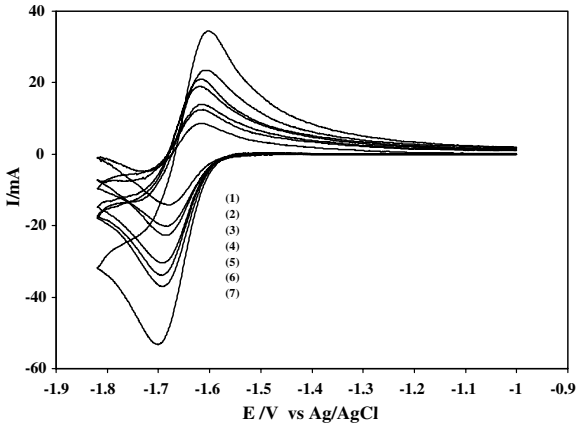

Fig. 2. Cyclic voltammograms of a $GdCl_3$ (9.0841×10^{-5} mol cm^{-3}) solution at 723 K at a Cd pool electrode after subtraction of the current background. Sweep rates: (1) 10, (2) 20, (3) 30, (4) 50, (5) 70, (6) 100 and (7) 200 mV s^{-1}.

The main characteristics of the voltammograms in Fig. 2 are the following: (i) the cathodic and anodic peak currents increase with the square root of the sweep rate – the regression analysis of the data give a R^2 of 0.989 and 0.988 which indicate a positive correlation of the values, and the residual analysis show that this correlation is compatible with a linear model – indicating that during the electrodepositon/reoxidation processes we encounter mass transport controlled by diffusion. (ii) Despite that the oxidized RE(III) and reduced RE species are moving in two different media of different properties, the ratio of the anodic and cathodic peak currents, I_{p_a}/I_{p_c}, remained close to unity, irrespective of the sweep rate. (iii) After correction of the ohmic drop, the cathodic and anodic peak potential values, E_p^c and E_p^a, do not change with increasing sweep rate for values comprised between 10 and 100 mV/s, whereas for higher sweep rates a slightly shift towards more cathodic and anodic values, respectively, is observed.

Taken into account the previous considerations, it is possible to calculate the reversible half-wave potential from the cyclic voltammograms obtained at sweep rates lower than 100 mV/s (i.e. reversible conditions) by means of Eq. (2) [11,12]:

$$E_{1/2} = \frac{E_{p_a} + E_{p_c}}{2} \quad (2)$$

or by simulation of the experimental curves [8,9,13,14] by the M271 COOl kinetic analysis software 1.10. The simulation method is based upon non-linear simplex optimization of the parameters in a normalized space derived from linear regression of the measured current on a calculated dimensionless current function [13,14]. A representative example of this simulation is shown in Fig. 3.

3.1.2. Estimation of the activity coefficients, partial molar enthalpy of mixing and partial molar excess entropy of RE in liquid Cd and Bi

According to Kurata et al. [15], it is possible to evaluate the excess Gibbs energy change of RE in

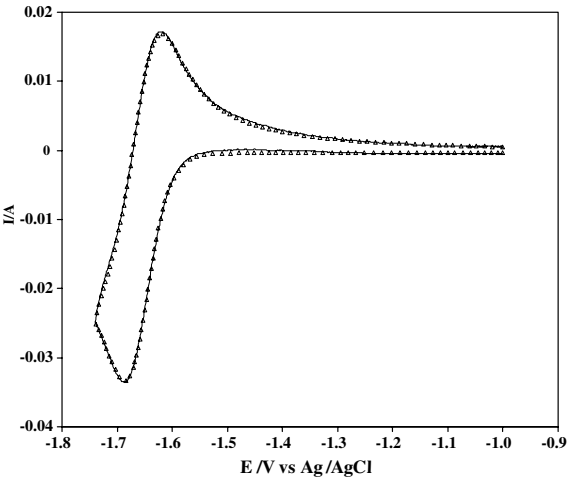

Fig. 3. Cyclic voltammogram of $GdCl_3$ reduction at a Cd pool electrode (sweep rate: 60 mV s^{-1}). (—) Experimental results; (△) simulated results.

liquid M, ΔG^{exc} (RE in M), and hence the activity coefficient of RE in liquid M, $\gamma_{RE\,in\,M}$, by measuring the electromotive force of the cell:

$$RE(0)|RE(III)\text{ in LiCl–KCl}|RE\text{ (in M)} \tag{3}$$

using Eq. (4):

$$\begin{aligned}\Delta G^{exc}(RE\text{ in M}) &= RT\ln\gamma_{RE\,in\,M}\\ &= -3F\Delta E - RT\ln x_{RE\,in\,M}.\end{aligned} \tag{4}$$

Considering the particular situation in which the concentration of RE(III) in solution is equal to the concentration of RE, in the metal phase, both concentrations expressed in mol cm^{-3}, the calculated reversible half-wave potential represents the equilibrium potential adopted by the liquid metal electrode

$$\begin{aligned}E^{eq}_{RE\,in\,M} &= E^{r}_{1/2} - (RT/3F)\\ &\quad\times\ln\left(D_{RE\,in\,M}/D_{RE(III)\,in\,LiCl–KCl}\right)^{1/2}\\ &\quad + RT/3F\ln\left[C_{RE(III)\,in\,LiCl–KCl}/C_{RE\,in\,M}\right]\\ &\quad\cong E^{r}_{1/2}.\end{aligned} \tag{5}$$

Therefore, ΔE, can be evaluated by means of Eq. (6)

$$\Delta E = E^{eq}_{RE\,in\,M} - E^{eq}_{RE} = E^{r}_{1/2} - E^{eq}_{RE}. \tag{6}$$

Mol fraction of RE in the liquid metal, $x_{RE\,in\,M}$, in Eq. (4), has been calculated from $C_{RE\,in\,M}$, expressed in mol/cm^3 by means of Eq. (7):

$$x_{RE\,in\,M} = C_{RE\,in\,M}M_M/(\rho_M + C_{RE\,in\,M}M_M) \tag{7}$$

being ρ_M the specific mass of the liquid M metal, M_M the atomic mass of M(Cd or Bi), and $C_{RE\,in\,M}$, the RE concentration in the M liquid metal expressed in mol/cm^3.

Finally, ΔG^{exc} (RE in M), can be evaluated by means of Eq. (8)

$$\begin{aligned}\Delta G^{exc}(RE\text{ in M}) &= RT\ln\gamma_{RE\,in\,M}\\ &= -3F(E^{r}_{1/2} - E^{eq}_{RE})\\ &\quad - RT\ln(C_{RE\,in\,M}M_M\\ &\quad /(\rho_M + C_{RE\,in\,M}M_M))\\ &= -3F(E^{r}_{1/2} - E^{eq}_{RE})\\ &\quad - RT\ln(C_{RE(III)\,in\,LiCl–KCl}M_M\\ &\quad /(\rho_M + C_{RE(III)\,in\,LiCl–KCl}M_M)).\end{aligned} \tag{8}$$

Along the experiments, the E^{eq}_{RE} was measured with a tungsten electrode covered with an electrodeposit of RE obtained under potentiostatic electrolysis as it was done elsewhere [8,9].

Fig. 4 shows, as an example, the relationship between the inverse temperature and the logarithm of the activity coefficients of Gd and Ce in Cd and La in Bi using the methodology proposed in this work, and the values taken from the literature [15–21].

The partial molar enthalpy of mixing and the partial molar excess entropy, which are useful for estimating the variation in the separation factor with increasing temperature, were calculated from the estimated molar excess Gibbs energy of the solute RE by means of Eq. (9):

$$\Delta G^{exc}_{RE} = RT\ln\gamma^{\#}_{RE} = \Delta H^{mix}_{RE} - T\Delta S^{exc}_{RE} \tag{9}$$

some results are gathered in Table 1.

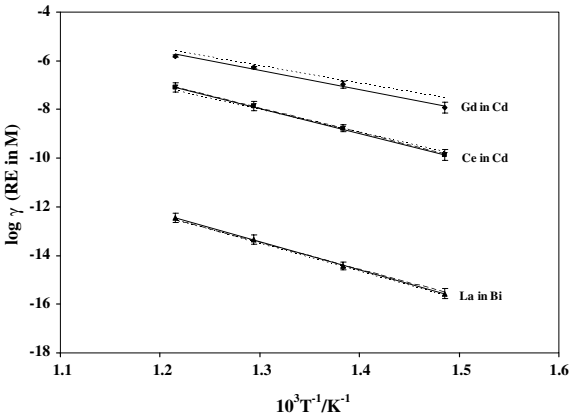

Fig. 4. Relationship between logarithms of activity coefficient of RE in M with inverse temperature. Gd in Cd: (◆) this work; (–––) [16]. Ce in Cd: (■) this work; (–––) [16]; (———) [17]. La in Bi: (▲) this work; (–––) [15]; (———) [21].

The good agreement between the results obtained by means of this methodology, with those taken from the literature, point out that it is possible to use electrochemical techniques, as a fast alternative approach, to estimate thermodynamic data.

3.2. Electrode reaction of the RE(III)/RE system at film electrodes

The phase diagrams of the RE–Cd and RE–Bi systems reported in the literature [22] show the presence of different intermetallic compounds. The alloying process can conveniently be studied by electrochemical techniques [8,9,23–25], for which Cd and Bi coated tungsten electrodes were used as working electrodes.

3.2.1. Results obtained by cyclic voltammetry

In Fig. 5 we have represented examples of cyclic voltammograms obtained with a $LaCl_3$ solution at a Cd film electrode. The voltammograms are more complex than those obtained at the pool electrode, and consist on a number of cathodic and anodic peaks corresponding to the formation–oxidation of different intermetallic compounds, mainly due to the different energies of formation of these phases rendering different formation–oxidation potentials.

The most important difference between the pools and the film electrodes is the smaller volume of the latter. As a result of this the concentration of RE in the liquid film electrode becomes much greater than the concentration of RE(III) in LiCl–KCl. The diffusion layer is larger in the liquid metal pool that in the film electrode, hence the film offers a limited or finite layer for the diffusion of metals and the semi-infinite diffusion model is no longer valid, moreover due to the small amount of M (Cd or Bi) in the film it might be formed distinct non-homogeneous phases during deposition.

Table 1
Partial molar enthalpy of mixing and partial molar excess entropy of solutes

Solvent	Solute	ΔH^{mix}	ΔS^{exc}	References
Cd	Pr	−172.0	−73.8	This work
	Pr	−178.2	−82.9	[16]
	Pr	−189.9	−99.2	[17]
	Ce	−195.4	−101.7	This work
	Ce	−178.7	−79.3	[16]
	Ce	−193.0	−99.0	[17]
	Gd	−149.1	−71.2	This work
	Gd	−134.8	−56.9	[16]
	Er	−128.18	−75.5	This work
Bi	Pr	−227.1	−51.9	This work
	Pr	−207.8	−23.6	[15]
	Pr	−228.6	−55.7	[18]
	Pr	−237.4	−63.3	[19]
	Ce	−216.9	−30.8	This work
	Ce	−209.8	−23.4	[15]
	Ce	−218.3	−38.9	[20]
	La	−222.4	−31.8	This work
	La	−219.8	−27.3	[15]
	La	−209.8	−14.9	[21]

3.2.2. Results obtained by open circuit chronopotentiometry

Open-circuit chronopotentiometry was carried out to investigate the alloy formation. The measurements were conducted as follows: (i) firstly, either RE metal is electrodeposited at a freshly formed Cd or Bi film electrode, or RE and the liquid Cd or Bi metal are both deposited, forming an intermetallic compound at a W electrode by potentiostatic electrolysis for a short period, (ii) afterwards, a transient curve of the open circuit potential was measured.

The equilibrium potentials measured by reference to the Ag|AgCl couple were converted to the electromotive forces (emf) against RE(0), which was prepared by electrodepositing RE metal on a pure *W* wire, making it possible to estimate the

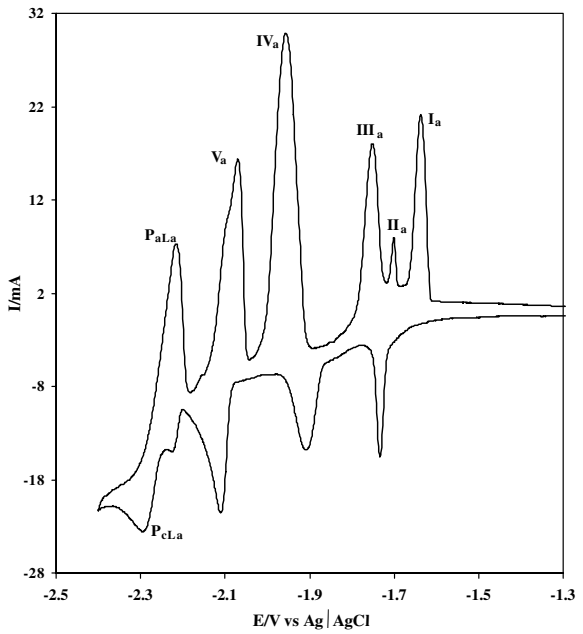

Fig. 5. Cyclic voltammograms for the reduction of a $LaCl_3$ (1.1385×10^{-4} mol cm^{-3}) solution at a Cd film electrode ($v = 50$ mV s^{-1}). $T = 748$ K.

Gibbs energies of formation of the intermetallic compounds [8,9,23–25].

Fig. 6 shows an example of the open circuit potential transient curves for a CdFE after depositing La metal by potentiostatic electrolysis at 693 K. Since the deposited RE metal reacts with the Cd and diffuses into the bulk of the film thickness, the electrode potential gradually shifts to more positive values. During this process, several potential plateaux are observed, which corresponds to a two phase coexisting state.

The emf corresponding to a chemical composition of the alloy is related to the activity of RE, a_{RE}, by the expression:

$$\mathrm{emf} = -(RT/3F)\ln a_{\mathrm{RE\ in\ M}}. \quad (10)$$

When the electrode surface is composed of a mixture of alloys of definite compositions $\mathrm{RE}_{x_1}\mathrm{M}$ and $\mathrm{RE}_{x_2}\mathrm{M}$, the activity of RE is fixed by the equilibrium:

$$\mathrm{RE}_{x_1}\mathrm{M} + (x_2 - x_1)\mathrm{RE} \leftrightarrow \mathrm{RE}_{x2}\mathrm{M} \quad (11)$$

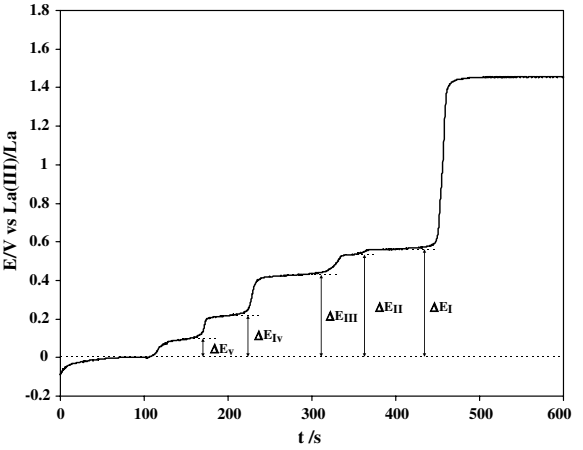

Fig. 6. Open circuit transient curve for a cadmium film electrode after electrodepositing La metal at −2.4 V vs. Ag|AgCl for 60 s at 748 K.

and so the emf has a constant value during the complete transformation of the definite alloy

Table 2
Thermodynamic properties of La for La–Cd intermetallic compounds in two-phase coexisting states at various temperatures

T/K	E/V vs. La(III)/La	$\Delta\overline{G}_{\mathrm{La}}$/kJ (mol La)$^{-1}$	a_{La}
In the two-phase coexisting state between LaCd and $LaCd_2$			
693	0.130 ± 0.007	−37.6 ± 2.0	$[1.53 \pm 0.5]\times 10^{-3}$
723	0.108 ± 0.003	−31.2 ± 0.7	$[5.65 \pm 0.7]\times 10^{-3}$
748	0.096 ± 0.012	−27.8 ± 3.5	$[1.15 \pm 0.5]\times 10^{-2}$
773	0.095 ± 0.005	−27.5 ± 1.4	$[1.41 \pm 0.3]\times 10^{-2}$
823	0.085 ± 0.005	−24.6 ± 1.4	$[2.79 \pm 0.6]\times 10^{-2}$
In the two-phase coexisting state between $LaCd_2$ and $La_{13}Cd_{58}$			
693	0.250 ± 0.004	−72.4 ± 1.2	$[3.60 \pm 0.7]\times 10^{-6}$
723	0.238 ± 0.004	−68.8 ± 1.0	$[1.10 \pm 0.2]\times 10^{-5}$
748	0.217 ± 0.005	−62.8 ± 1.4	$[4.14 \pm 0.9]\times 10^{-5}$
773	0.209 ± 0.006	−60.4 ± 1.8	$[8.58 \pm 2.6]\times 10^{-5}$
823	0.204 ± 0.013	−59.0 ± 3.8	$[2.04 \pm 1.1]\times 10^{-4}$
In the two-phase coexisting state between $La_{13}Cd_{58}$ and La_2Cd_{17}			
693	0.459 ± 0.021	−132.8 ± 6.2	$[1.49 \pm 1.2]\times 10^{-10}$
723	0.444 ± 0.009	−128.5 ± 2.7	$[5.71 \pm 2.2]\times 10^{-10}$
748	0.425 ± 0.010	−123.0 ± 2.9	$[2.60 \pm 1.0]\times 10^{-9}$
773	0.423 ± 0.004	−122.6 ± 1.2	$[5.37 \pm 0.9]\times 10^{-9}$
823	0.411 ± 0.010	−118.9 ± 2.9	$[3.11 \pm 1.2]\times 10^{-8}$
In the two-phase coexisting state between La_2Cd_{17} and $LaCd_{11}$			
693	0.555 ± 0.019	−160.7 ± 5.5	$[7.94 \pm 4.9]\times 10^{-13}$
723	0.541 ± 0.020	−156.6 ± 5.8	$[4.95 \pm 3.1]\times 10^{-12}$
748	0.533 ± 0.015	−154.3 ± 4.3	$[1.71 \pm 0.9]\times 10^{-11}$
773	0.512 ± 0.012	−148.2 ± 3.5	$[9.83 \pm 4.2]\times 10^{-11}$
823	0.478 ± 0.010	−138.4 ± 2.9	$[1.68 \pm 0.6]\times 10^{-9}$
In the two-phase coexisting state between $LaCd_{11}$ and Cd			
693	0.587 ± 0.027	−169.9 ± 7.7	$[3.48 \pm 4.6]\times 10^{-13}$
723	0.569 ± 0.014	−164.7 ± 4.0	$[1.65 \pm 1.6]\times 10^{-12}$
748	0.560 ± 0.014	−162.1 ± 4.1	$[4.88 \pm 2.3]\times 10^{-12}$
773	0.534 ± 0.004	−154.7 ± 1.0	$[3.62 \pm 0.6]\times 10^{-11}$
823	0.508 ± 0.014	−147.0 ± 4.1	$[5.48 \pm 2.8]\times 10^{-10}$

Table 3
Gibbs energies of formation for La–Cd intermetallic compounds

Reaction of alloy formation	Equation	T/K	ΔG_f^0/kJ mol^{-1}
$La + 11Cd \leftrightarrow LaCd_{11}$	$\Delta G^0_{f,LaCd_{11}} = -3F\Delta E_I$	693	-169.9 ± 7.7
		723	-164.7 ± 4.0
		748	-162.1 ± 4.1
		773	-154.7 ± 1.0
		823	-147.0 ± 4.1
$La + 8.5Cd \leftrightarrow LaCd_{8.5}$	$\Delta G^0_{f,LaCd_{8.5}} = \frac{2.5}{11}\left[\frac{8.5}{2.5}\Delta G^0_{f,LaCd_{11}} - 3F\Delta E_{II}\right]$	693	-167.8 ± 1.3
		723	-162.9 ± 1.3
		748	-160.3 ± 1.0
		773	-153.2 ± 0.8
		823	-145.0 ± 0.7
$La + 4.46Cd \leftrightarrow LaCd_{4.46}$	$\Delta G^0_{f,LaCd_{4.46}} = \frac{4.04}{8.5}\left[\frac{4.46}{4.04}\Delta G^0_{f,LaCd_{8.5}} - 3F\Delta E_{III}\right]$	693	-151.2 ± 2.9
		723	-146.5 ± 1.2
		748	-142.6 ± 1.4
		773	-138.6 ± 0.6
		823	-132.6 ± 1.4
$La + 2Cd \leftrightarrow LaCd_2$	$\Delta G^0_{f,LaCd_2} = \frac{1.23}{2.23}\left[\frac{1}{1.23}\Delta G^0_{f,LaCd_{4.46}} - 3F\Delta E_{IV}\right]$	693	-107.7 ± 0.7
		723	-103.6 ± 0.6
		748	-98.6 ± 0.8
		773	-95.5 ± 1.0
		823	-92.0 ± 2.1
$La + Cd \leftrightarrow LaCd$	$\Delta G^0_{f,LaCd} = \frac{1}{2}\left[\Delta G^0_{f,LaCd_2} - 3F\Delta E_V\right]$	693	-72.7 ± 1.0
		723	-67.4 ± 0.4
		748	-63.2 ± 1.7
		773	-61.5 ± 0.7
		823	-58.3 ± 0.7

$RE_{x_1}M$ into the definite alloy $RE_{x_2}M$. For the exact composition of a definite alloy, $RE_{x_2}M$ for example, we observe a variation of the emf from the value of the two phase plateaux corresponding to the mixture of $RE_{x_1}M$ and $RE_{x_2}M$ to the value of the two phase plateau of $RE_{x_2}M$ and $RE_{x_3}M$ mixture.

The standard Gibbs energies of formation ΔG_f^0 of an alloy of composition $RE_{x_2}M$ is related to that of a RE_{x1} alloy by

$$\Delta G_f^0(RE_{x_2}M) = -3F\int_{x_1}^{x_2} \Delta E(x)\,dx + \Delta G_f^0(RE_{x_1}M). \quad (12)$$

Table 4
Enthalpies and entropies of formation of cadmium and bismuth rich alloys in RE–Cd and RE–Bi systems

Compound	ΔH_f^0/kJ mol^{-1}	ΔS_f^0/J mol^{-1} K^{-1}
$PrCd_{11}$ [8]	-291.8 ± 13.5	-192.3 ± 18.0
$CeCd_{11}$	-275.4 ± 33.2	-163.4 ± 45.5
$LaCd_{11}$	-294.0 ± 21.5	-179.2 ± 20.5
$GdCd_6$	-205.7 ± 11.6	-110.4 ± 15.6
$ErCd_6$	-146.5 ± 3.6	-49.0 ± 4.7
$CeBi_2$ [9]	-274.0 ± 2.9	-71.4 ± 3.8
$PrBi_2$ [8]	-257.7 ± 11.3	-46.3 ± 15.1

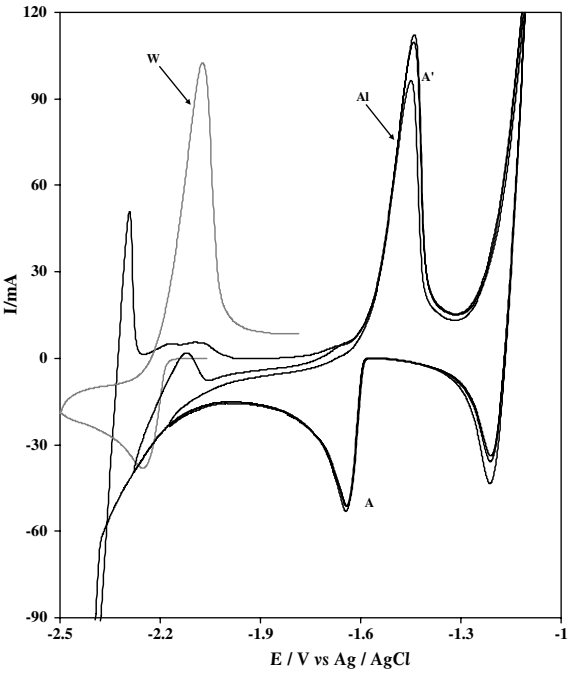

Fig. 7. Cyclic voltammograms for the reduction of a $CeCl_3$ solution at an Al electrode (black lines) and at a W electrode (grey line) at 723 K. Scan rate: 0.1 V s^{-1}.

The results obtained in the case of La–Cd compounds are gathered in Tables 2 and 3.

The enthalpies and entropies of formation of the intermetallic compounds have been calculated from the variation of the energy of formation of the different intermetallic compounds with the temperature. The results for the Cd and Bi rich alloys in the RE–Cd and RE–Bi systems are gathered in Table 4.

3.3. Electrode reactions of RE(III)/RE system at an Al electrode

3.3.1. Results obtained by cyclic voltammetry

In Fig. 7 we have compared the cyclic voltammograms obtained at a W and Al electrodes in the case of gadolinium, as an example of RE metal electrodeposition. For the Al electrode, a cathodic peak A is observed at a potential more positive than those for RE metal deposition onto W, due to a lowering of activity of the deposited metal in the Al phase. Therefore, the cathodic peak A is thought to be caused by the formation of a RE–Al alloy. When the scanning direction is reversed, an anodic peak A′ is observed previously to the Al oxidation, which corresponds to the RE oxidation from the RE–Al alloy.

Based on the previous results, potentiostatic electrolysis of a solution of $RECl_3$ using an aluminium foil was conducted at a potential value more positive than the pure RE metal deposition potential,

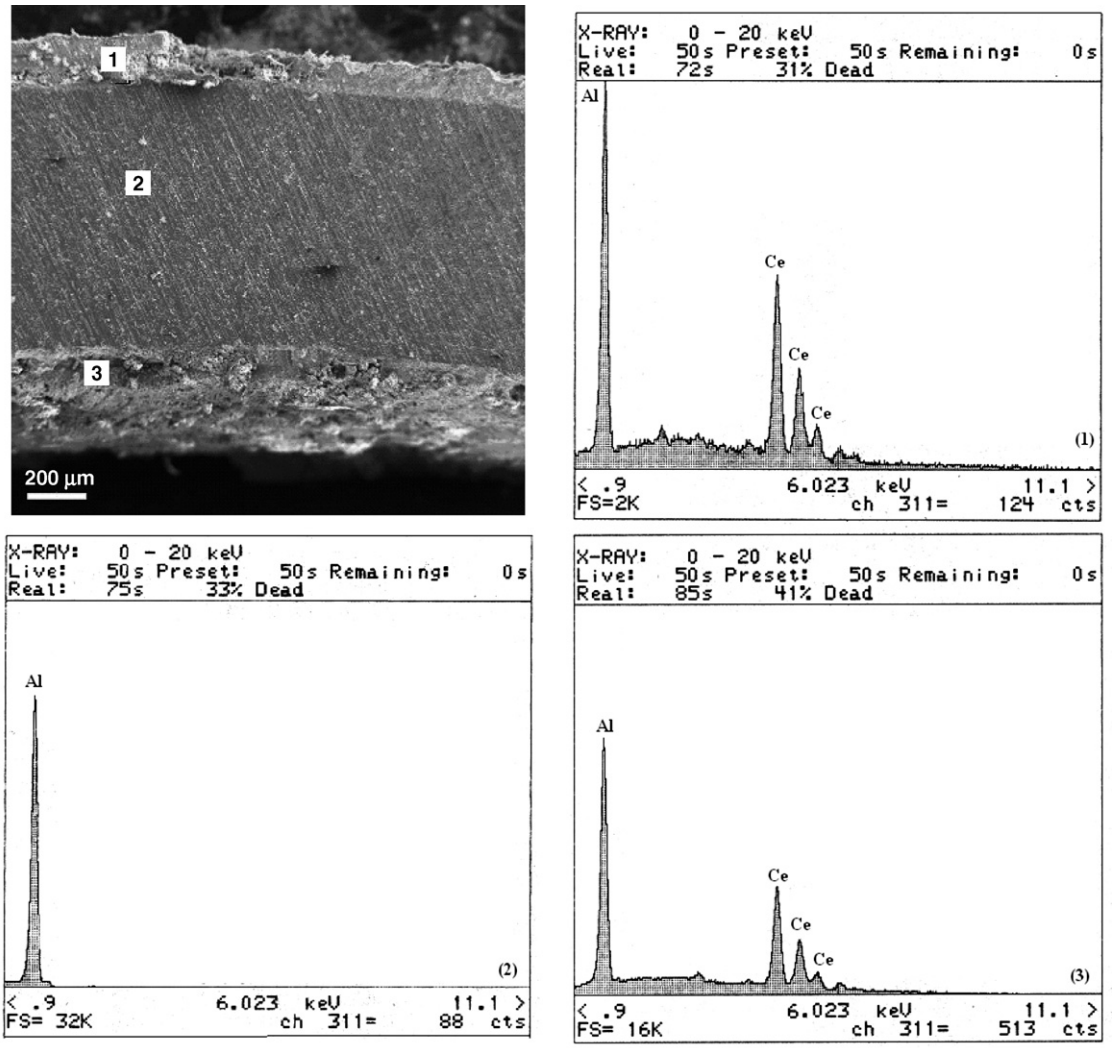

Fig. 8. Cross-sectional SEM image of a Ce–Al film formed by potentiostatic electrolysis at −1.9 V vs. Ag|AgCl, and EDX analysis corresponding to points (1), (2) and (3).

using an aluminium foil as working electrode. After the electrolysis, the samples were washed by anhydrous ethylene glycol (Aldrich 99.8%) and stored inside the glove box until their analysis. The surface of the samples were analysed by XRD and EDX, and the surface morphology of the deposits was observed by scanning electron microscopy (SEM). Some examples are shown in Figs. 8 and 9.

3.3.2. Analysis of the open circuit chronopotentiograms

Open circuit chronopotentiometry was also carried out to investigate the thermodynamics of the aluminium rich alloys in the RE–Al system. The measurements were conducted in a similar way than in the case of the Cd and Bi film electrodes, (i) a constant potential was applied at the aluminium electrode, (ii) then a transient curve of the open circuit potential was recorded (Fig. 10). During this process, a potential plateau is observed when a composition of the electrode surface is within a range of two phase coexisting state.

The equilibrium potentials of the potential plateaux were converted to electromotive forces (emf) against RE(0), which allows us to estimate the Gibbs energies of formation of the intermetallic compounds and the activity of the REs in the intermetallic compounds. The molar entropies and enthalpies of formation of the aluminium rich alloys are gathered in Table 5.

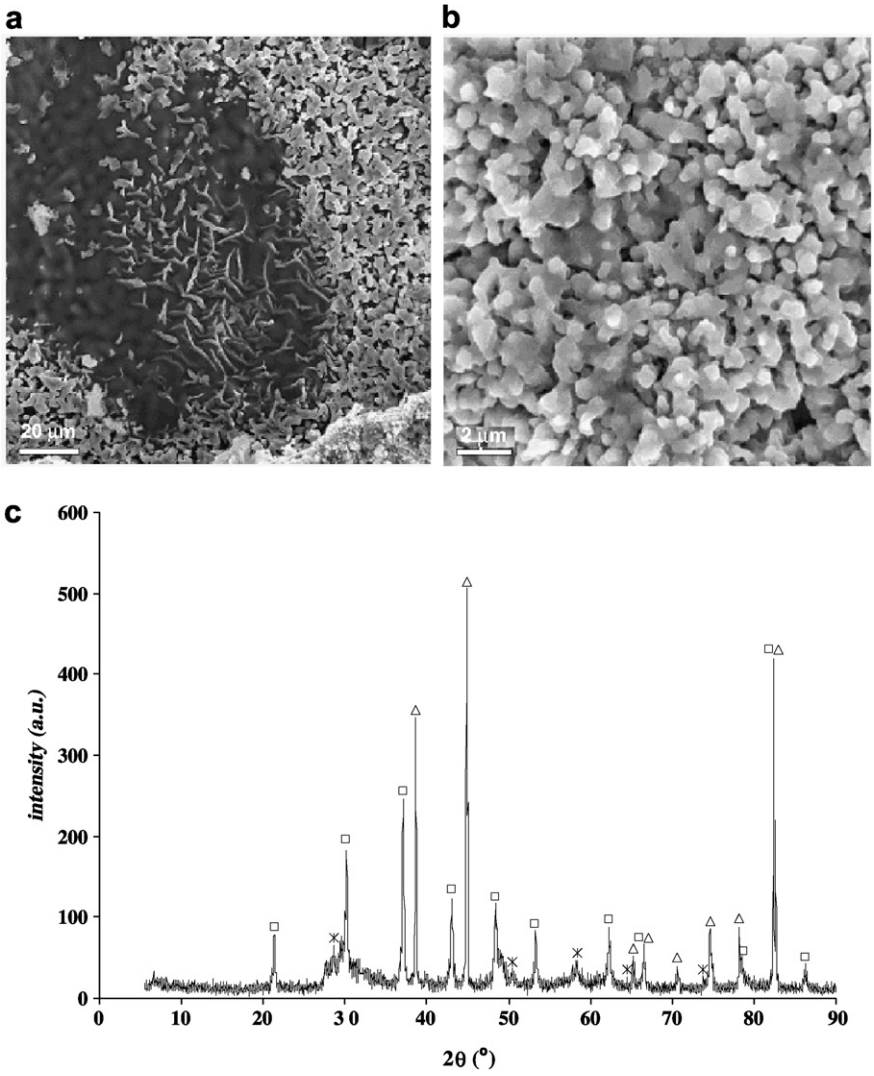

Fig. 9. SEM micrographs of Al cathode covered by $ErAl_3$deposit: (a) and (b) details, (c) X-ray diffraction analysis: (□) Al_3Er, (△) Al, (∗) KCl.

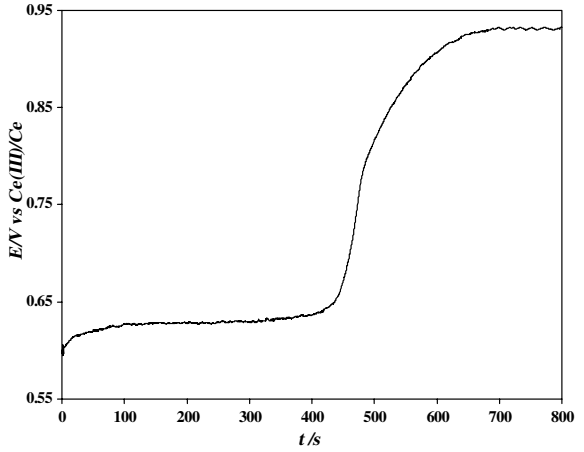

Fig. 10. Open circuit transient curve for an Al electrode after electrodepositing Ce at −2.0 V vs. Ag|AgCl for 5 s at 723 K.

Table 5
Enthalpies and entropies of formation of aluminium rich alloys in RE–Al systems

Compound	ΔH_f^0/kJ mol^{-1}	ΔS_f^0/J mol^{-1} K^{-1}
$Al_{11}Pr_3$ [26]	−212.3	−45.2
$Al_{11}Ce_3$	−208.5	−38.8
$Al_{11}La_3$	−205.2	−34.5
Al_3Gd [28]	−193.82	−43.9
Al_3Y	−187.7	−40.2
Al_3Er [27]	−176.4	−29.9
Al_3Ho	−191.4	−49.8

4. Conclusions

The electrode reaction of the RE(III)/RE couples at the liquid Cd and Bi electrodes were elucidated by electrochemical techniques. The redox potential of the RE(III)/RE couples at the liquid electrode were observed at more positive potential values than those at an inert electrode (W). This potential shift was thermodynamically explained by a lowering of activity of REs in the metal phase due to the formation of intermetallic compounds. The values of the reversible half wave potential, $E^r_{1/2}$, have been obtained by simulation of the cyclic voltammograms at the liquid pool electrodes.

Because of the ease of application of cyclic voltammetry, it was suggested as a general method to obtain approximate values of the excess Gibbs energy change of REs in the liquid metals, and hence of the activity coefficients, $\gamma_{RE\,in\,M}$, the partial molar enthalpy of mixing and the partial molar excess entropy. The estimated values were obtained from comparison between the equilibrium potential adopted by a RE electrode immersed in a solution containing RE(III) ions, and the calculated $E^r_{1/2}$ of the system RE(III)/RE–M in the experiments conducted with the same RE(III) solution. The results obtained along this study are in good agreement with those of the literature [15–21].

Cyclic voltammetry and open circuit chronopotentiometry measurements using Cd and Bi film electrodes were also conducted. Due to the small volume of the film electrodes, the electroreduction of RE(III) on film electrodes proceeds via the formation of distinct non-homogeneous phases.

Electromotive force, emf, measurements for various intermetallic compounds in two-phase coexisting states were carried out in the temperature range of 673–823 K. The activities and relative partial molar Gibbs energies of REs were obtained from the measured emf values for different intermetallic compounds. The molar entropies and enthalpies of formation for the RE–Cd and RE–Bi intermetallic compounds were also calculated from the temperature dependence of the emf values.

Cyclic voltammetry and open circuit chronopotentiometry measurements have proven that REs forms alloys with solid Al electrodes. The electroreduction of RE(III) ions on Al proceeds via the formation of a stable RE–Al alloy.

emf measurements for the RE–Al intermetallic compounds coexisting in two-phase states were carried out at temperatures comprised between 673 and 823 K. The activity of REs, in the Al phase, as well as the standard Gibbs energy of formation, enthalpies and entropies of the aluminium rich alloys were estimated from these measurements.

Acknowledgements

The authors would like to thank ENRESA (Spain) (CIEMAT-ENRESA and CIEMAT-UNIVERSIDAD DE VALLADOLID agreements) for their financial support of some aspects of the study, and the Ministerio de Educación y Ciencia MEC-FEDER (Spain) Project ENE2004-00317/CON for the financing of other parts. We would also like to indicate that some aspects of the work were part of the UE PYROREP FIKW-CT-2000-00049 project.

References

[1] H.P. Nawada, K. Fukuda, J. Phys. Chem. Solids 66 (2005) 647.
[2] Y.I. Chang, Nucl. Technol. 88 (1989) 129.

[3] T. Koyama, M. Iizuka, H. Tanaka, M. Tokiwai, Y. Shoji, R. Fujita, T. Kobayashi, J. Nucl. Sci. Technol. 34 (1997) 384.
[4] K. Uozomi, M. Iizuka, T. Kato, T. Inoue, O. Shirai, T. Iwai, Y. Arai, J. Nucl. Mater. 325 (2004) 34.
[5] M. Iizuka, K. Uozomi, T. Inoue, T. Iwai, O. Shirai, Y. Arai, J. Nucl. Mater. 299 (2001) 32.
[6] O. Shirai, M. Iizuka, T. Iwai, Y. Arai, Anal. Sci. 17 (2001) 51.
[7] O. Shirai, M. Iizuka, T. Iwai, Y. Suzuki, Y. Arai, J. Electroanal. Chem. 490 (2000) 31.
[8] Y. Castrillejo, M.R. Bermejo, P. Díaz Arocas, A.M. Martínez, E. Barrado, J. Electroanal. Chem. 579 (2005) 343.
[9] Y. Castrillejo, M.R. Bermejo, P. Díaz Arocas, F. De la Rosa, E. Barrado, Electrochemistry 73 (8) (2005) 636.
[10] M.A. Lewis, T.R. Johnson, J. Electrochem. Soc. 137 (1990) 1414.
[11] M. Noel, K.I. Vasu, Cyclic Voltammetry and the Frontiers of Electrochemistry, Oxford & IBH Publishing Co. Pvt. Ltd., New Delhi, 1990.
[12] A.J. Bard, L.R. Faulkner, Electrochemical Methods Fundamentals and Applications, Wiley, New York, 2001.
[13] J. O'Dea, J. Osteryoung, R. Osteryoung, J. Phys. Chem. 87 (1983) 3911.
[14] J. O'Dea, J. Osteryoung, J. Phys. Chem. 90 (1986) 2761.
[15] M. Kurata, Y. Sakamura, T. Matsui, J. Alloys Compd. 234 (1996) 83.
[16] Y. Sakamura, T. Inoue, T.S. Storvick, L.F. Grantham, in: Proceedings of the Molten Salt Chem. Soc., Sapporo, 1994, p. 101 (in Japanese).
[17] I. Jhonson, R.M. Yonco, Metall. Trans. 1 (1970) 905.
[18] V.I. Kober, V.A. Dybinin, S.P. Raspopin, S.R. Kanevski, Izv. Vyz. Tsvet. Metall. 5 (1985) 109.
[19] V.A. Lebedev, Selectivity of Liquid Metal Electrodes in Molten Halides, Cheliyabinsk Metallyrgiya, Cheliyabinsk, 1993.
[20] V.I. Kober, V.A. Lebedev, I.F. Nichkov, S.P. Raspopin, Russ. J. Phys. Chem. 45 (1971) 313.
[21] V.I. Kober, V.A. Lebedev, I.F. Nichkov, S.P. Raspopin, Russ. J. Phys. Chem. 42 (1968) 360.
[22] T.B. Massalski (Ed.), Binary Alloy Phase Diagrams, ASM International, Materials Park, OH, 1990.
[23] G.S. Picard, Y.E. Mottot, B.L. Trémillon, Proceedings of the Fourth International Symposium on Molten Salt, vol. 84 (2), The Electrochem. Soc., 1984, p. 585.
[24] P. Taxil, J. Mahenc, J. Appl. Electrochem. 17 (1987) 261.
[25] H. Konishi, T. Nishikiori, T. Nohira, Y. Ito, Electrochim. Acta 48 (2003) 1403.
[26] Y. Castrillejo, M.R. Bermejo, P. Díaz Arocas, A.M. Martínez, E. Barrado, J. Electroanl. Chem. 575 (2005) 61.
[27] Y. Castrillejo, M.R. Bermejo, E. Barrado, A.M. Martínez, Electrochim. Acta 51 (2006) 1941.
[28] Y. Castrillejo, M.R. Bermejo, J. Gómez, J. Medina, A.M. Martínez, J. Electronal. Chem. 588 (2006) 253.